11

Optical properties of van der Waals heterostructures based on 2D monolayers of borophene, gallium nitride, and zinc oxide

© M.M. Slepchenkov, D.A. Kolosov, O.E. Glukhova

Saratov National Research State University, Saratov, Russia

e-mail: slepchenkovm@mail.ru

Received December 20, 2022
Revised January 19, 2023
Accepted February 06, 2023

In this paper, we consider two new atomic models of van der Waals vertical heterostructures of metal-semiconductor type based on a 2D buckled triangular borophene with metallic conductivity and graphene-like 2D monolayers of gallium nitride GaN and zinc oxide ZnO, which are semiconductors. Using the density functional theory, the equilibrium configurations of supercells of the borophene/GaN and borophene/ZnO heterostructures are found and their thermodynamic stability at room temperature is shown. Within the framework of the nonstationary first-order perturbation theory, the optical characteristics (complex permittivity and absorption coefficient) are calculated in the electromagnetic radiation wavelength range of $0.2-2\,\mu$mm. The presence of anisotropy in the optical properties of the borophene/GaN and borophene/ZnO heterostructures is established when the direction of light polarization is chosen. This is due to different manifestations of the optical properties of the constituent monolayers of the heterostructure. When light is polarized in the direction of the zigzag edge of the GaN/ZnO (along the X axis), the optical properties of GaN and ZnO semiconductor monolayers are predominantly manifested. When light is polarized in the direction of the zigzag edge of the borophene monolayer (along the Y axis), the optical properties of borophene manifest themselves. A synergistic effect has been found from the combination of borophene and ZnO monolayers in the composition of the borophene/ZnO vertical heterostructure, which manifests itself in the form of a section of the increasing plot of the real and imaginary parts of the complex permittivity in the infrared region for both directions of light polarization. It is shown that the difference in the values of the absorption coefficient of the borophene/GaN heterostructure between the UV and visible ranges can reach 7 times, between the UV and near IR ranges - 14 times, and for the borophene/ZnO heterostructure this difference can be up to 6 times and up to 18 times, respectively. It is predicted that borophene/GaN and borophene/ZnO heterostructures can be used to create UV radiation detectors.

Keywords: van der Waals vertical heterostructures, complex permittivity, absorption coefficient, anisotropy of optical properties.

DOI: 10.61011/EOS.2023.06.56658.115-23

1. Introduction

The stacking of 2D crystals with atomic thickness with different types of conductivity in the form of a vertical heterostructure opens wide opportunities to produce new nanomaterials with unique properties [1,2]. Due to the fact that 2D crystals in such layered heterostructures are bound only by weak van der Waals forces, it becomes possible to combine atomically thin membranes with large differences in lattice parameters and even with completely different crystal structures [3]. To form vertical heterostructures, such 2D materials as graphene, boron nitride, zinc oxide, as well as various representatives of the groups of transition metal dichalcogenides (TMD), transition metal carbides and nitrides (MXenes), and organometallic compounds are widely used [4–9]. A wide variety of electronic and optical properties of the above-mentioned 2D materials determines the prospects for the use of van der Waals heterostructures based on them in the creation of various nanoelectronic and optoelectronic devices [10–12]. In particular, the ultrafast charge transfer characteristic of van der Waals heterostructures makes them a promising material for photosensitive elements of optoelectronic devices. Solar cells based on TMD heterostructures, mainly molybdenum disulfide MoS_2 and diselenide $MoSe_2$, as well as tungsten disulfide WS_2 and diselenide WSe_2, have already been developed [13–15]. In the development of UV radiation photodetectors, metal oxides are used, for example, zinc oxide ZnO and titanium dioxide TiO_2, as well as representatives of group III nitrides, such as gallium nitride GaN, aluminum nitride AlN, indium nitride InN [16]. The most popular type of UV radiation sensor is a device based on a photodiode with a Schottky barrier, which is formed in heterostructures of the metal-semiconductor type [17–23]. Currently, van der Waals heterostructures based on graphene, MoS_2, $MoSe_2$, $MoTe_2$ are extensively used for the manufacture of metal-semiconductor contacts [21–23]. With the successful synthesis of borophene, a 2D material consisting entirely of boron atoms [24], the possibility of implementing a metal-semiconductor contact on borophene heterostructures began to be discussed [25–27]. In particular, based on the results of ab initio calculations, it is prognosed that van der Waals

heterostructures of the borophene type β_{12}/MX_2 (M = Mo, W and X = S, Se) [25], borophene/InSe [26], borophene/g-C2N [27] can be used to develop contacts with a Schottky barrier. A distinctive feature of these heterostructures is the ability to control the magnitude of the Schottky barrier due to tensile/compressive strain [25] and an external electric field [26,27].

This study considers two new configurations of van der Waals heterostructures of the metal-semiconductor type based on borophene: borophene/GaN and borophene/ZnO. The purpose of this work is to preliminary evaluate the optical properties of borophene/GaN and borophene/ZnO van der Waals heterostructures by ab initio methods.

2. Research methods

The van der Waals heterostructures were *ab initio* studied in the framework of the density functional theory (DFT) implemented in the SIESTA 4.1.5 software package [28]. To describe the exchange-correlation effects, a generalized gradient approximation (GGA) in the PBE parameterization (Perdew–Burke–Ernzerhof) was applied [29]. The van der Waals interaction between the layers of the heterostructure was described using the Grimme's dispersion correction (the DFT+D2 field of forces) [30]. The atomic structure of supercells was optimized until the change in the force acting on each atom became less than 0.025 eV/Å. In this process the DZ2P (double zeta 2 polarization) split-valence orbitals basis set, which includes polarization functions, was used. The energy of the electronic subsystem was minimized using the effective Broyden–Pulay mixing scheme [31]. To rule out the influence of the heterostructure layers on each other in the nonperiodic direction, the vacuum gap was no less than 20 Å. The cutoff energy was chosen to be 150 Ry. The Brillouin zone was divided using the Monkhorst–Pack method [32] with a k-point mesh size of $12 \times 6 \times 1$.

To study the optical properties of van der Waals heterostructures, the complex frequency-dependent permittivity was calculated in the SIESTA software package within the first-order non-stationary perturbation theory [33]. The imaginary part of the permittivity determines the optical absorption, which is calculated from the rate of transition between the occupied states of the valence band and the free states of the conduction band. The formula for calculating the absorption coefficient A is as follows:

$$A(\omega) = \frac{\omega}{cn(\omega)}\varepsilon_2(\omega), \tag{1}$$

where $\varepsilon_2(\omega)$ is the imaginary part of the complex permittivity, $n(\omega)$ is the refractive index, c is the speed of light. The $\varepsilon_2(\omega)$ is calculated by the following formula:

$$\varepsilon_2(\omega) = \frac{e^2}{\pi m^2 \omega^2} \sum_{v,c} \int_{BZ} dk \times |\langle \psi_{ck} | \hat{\mathbf{e}}, \mathbf{p} | \psi_{vk} \rangle|^2 \delta(E_c(k) - E_v(k) - \hbar\omega), \tag{2}$$

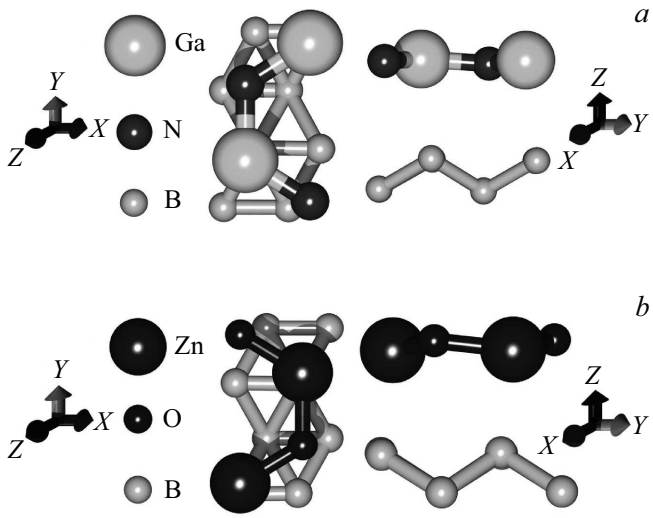

Figure 1. Atomic structure of supercells of borophene/GaN (*a*) and borophene/ZnO (*b*) van der Waals heterostructures.

where the summation is carried out over each pair of states of the valence (filled) band and the conduction band (unoccupied), and the integration is carried out over all k-points in the Brillouin zone, c and v subscripts refer to electronic states in the conduction and valence bands, respectively, $E_{c,v}(k)$ and $\phi_{(c,v),k}$ are energies and eigenfunctions of these states. The matrix element of the electronic dipole transition lies between the occupied and unoccupied states, where $\hat{\mathbf{e}}$ is the polarization vector, and $\mathbf{p}$ is the momentum operator. The optical parameters of the van der Waals heterostructures in question were calculated for two different directions of light polarization (the $\mathbf{E}$ vector parallel to the X axis and parallel to the Y axis) for the energy range from 0.6 to 20 eV using optical broadening of 0.05 eV. Optical characteristics of the studied heterostructures were calculated with the Brillouin zone divided into k-points with a mesh size of $114 \times 65 \times 1$.

3. Atomic structure of borophene/GaN and borophene/ZnO van der Waals heterostructures

Supercells of the van der Waals heterostructures under study were built using graphene-like sheets of GaN and ZnO, as well as a 2D corrugated borophene sheet with a triangular crystal lattice. Lattice cells of the GaN and ZnO monolayers were taken from the Materials Project open access database [34]. Their translation vectors are $L_x = 3.204$ Å, $L_y = 5.55$ Å for GaN and $L_x = 3.205$ Å, $L_y = 5.551$ Å for ZnO. The choice of the 2D structures of ZnO and GaN is explained by the close correspondence between their crystal lattice parameters and the crystal lattice of corrugated borophene, which makes it possible to significantly reduce the size of the atomic structures to be calculated. In addition, both GaN and ZnO have previ-

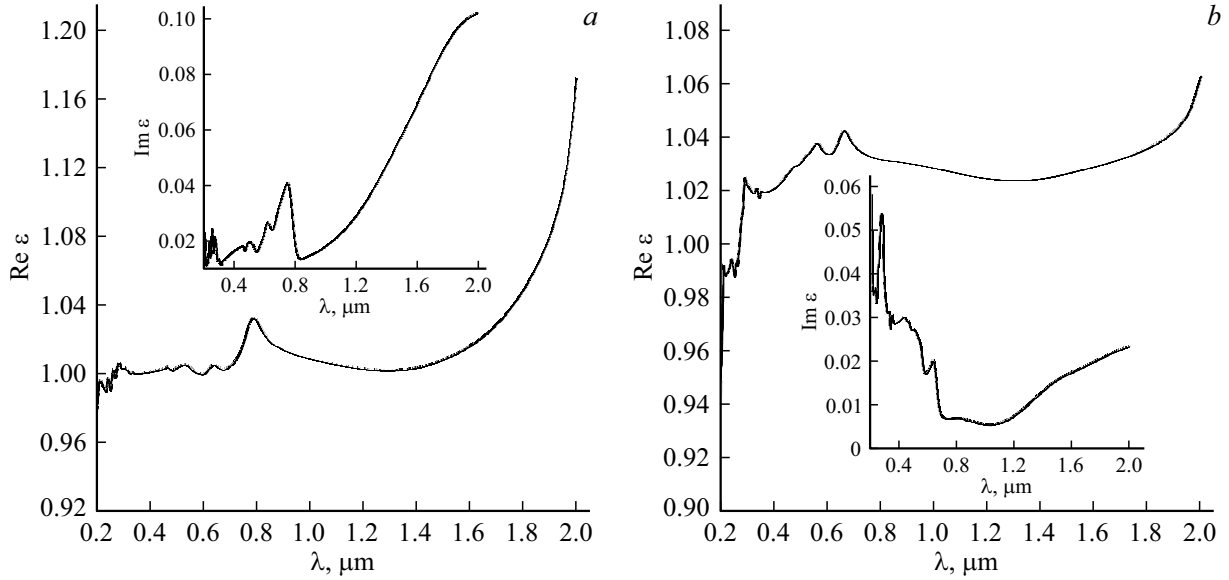

Figure 2. Dependences of the real Re and imaginary Im parts of the complex permittivity $\dot{\varepsilon}$ of the borophene/GaN heterostructure on the λ wavelength for two directions of light polarization: (a) along the X axis; (b) along the Y axis.

ously been successfully used in the building up graphene-based vertical heterostructures, which have demonstrated promising optoelectronic properties. [35,36]. The lattice cell of corrugated borophene was built taking into account the data of [37]. The translation vectors of this cell are $L_x = 1.613$ Å, $L_y = 2.864$ Å. The choice of corrugated borophene with a triangular crystal lattice among the existing allotropic forms of borophene is due to its high energy stability [38]. Fig. 1 shows supercells of borophene/GaN and borophene/ZnO van der Waals heterostructures (plan view and side view). Translation vectors of the optimized supercell for the borophene/GaN heterostructure were $L_x = 3.35$ Å, $L_y = 6.10$ Å, and these vectors for the borophene/ZnO were $L_x = 3.28$ Å, $L_y = 5.83$ Å. The distance between the borophene and GaN monolayers along the Z axis is 2.91 Å, and the distance between the borophene and ZnO layers is 2.51 Å.

For the built supercells of the borophene/GaN and borophene/ZnO heterostructures, the thermodynamic stability at room temperature was evaluated. The thermodynamic stability was evaluated from the bond energy, which was calculated as the difference between the total energy of the heterostructure and the total energy of isolated monolayers divided by the number of atoms in the supercell. According to the results of calculations, the bond energy for a supercell of borophene/GaN heterostructure is ~ -50 meV/atom, and for a supercell of borophene/ZnO it is ~ -80 meV/atom. The negative value of the bond energy indicates that the structures are energy stable and, therefore, can be implemented in practice. In addition, the bond energy of borophene/GaN and borophene/ZnO heterostructures is higher than that of a number of other heterostructures based on GaN and ZnO monolayers, for example, it is almost twice higher than the bond energy of MoSSe-g-GaN and WSSe-g-GaN [39] and more than 6 times higher than the bond energy of ZnO/g-GeC [40].

4. Optical properties of borophene/GaN and borophene/ZnO van der Waals heterostructures

The optical properties of the studied borophene/GaN and borophene/ZnO van der Waals heterostructures were analyzed on the basis of the calculated permittivity and absorption spectra in the wavelength range of $0.2-2\,\mu$m (UV, optical, and near-IR radiation ranges). The calculations were carried out for two directions of light polarization (along the X axis and the Y axis). Fig. 2 shows graphs of the real (Re) and imaginary (Im) parts of the complex permittivity $\dot{\varepsilon}$ of the borophene/GaN heterostructure depending on the wavelength of electromagnetic radiation λ. It can be seen from the presented dependences that when the light is polarized both along the X axis and along the Y axis, Re $\dot{\varepsilon}$ is dozens of times greater than Im $\dot{\varepsilon}$. Consequently, in the wavelength range in question, the borophene/GaN heterostructure manifests itself as a medium with dielectric properties. The patterns of Re $\dot{\varepsilon}$ change with increasing wavelength for both directions of light polarization are similar to each other, in contrast to the behavior of Im $\dot{\varepsilon}$. Along the X axis, the values of Im $\dot{\varepsilon}$ increase with the transition between the UV, visible and IR radiation ranges, while along the Y axis in the UV and visible radiation ranges the Im $\dot{\varepsilon}$ decreases nonmonotonically, and in the IR radiation range its smooth increase is observed. Accordingly, the maximum Im $\dot{\varepsilon}$ with the light polarization along the X axis is in the near-IR radiation range, and with the light polarization along the Y

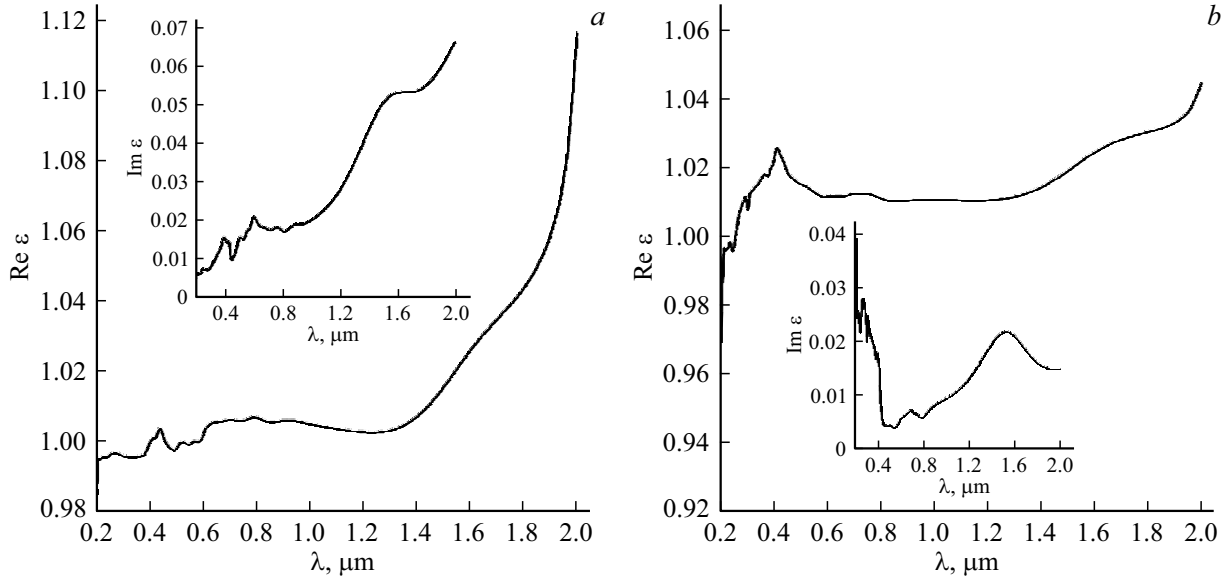

Figure 3. Dependences of the real Re and imaginary Im parts of the complex permittivity $\dot{\varepsilon}$ of the borophene/ZnO heterostructure on the λ wavelength for two directions of light polarization: (*a*) along the *X* axis; (*b*) along the *Y* axis.

axis it is in the UV radiation range. The observed differences indicate the presence of dielectric permittivity anisotropy for this structure, which should also affect the ability of the borophene/GaN heterostructure to absorb electromagnetic radiation, taking into account the direct relationship between Im $\dot{\varepsilon}$ and the absorption coefficient according to formula (1).

The dependences of Re $\dot{\varepsilon}$ and Im $\dot{\varepsilon}$ on the wavelength λ for the borophene/ZnO heterostructure are shown in Fig. 3. As in the case of the borophene/GaN heterostructure, Re $\dot{\varepsilon}$ differs from Im $\dot{\varepsilon}$ by dozens of times for both directions of light polarization; therefore, the borophene/ZnO heterostructure can be considered a medium with dielectric properties in the wavelength range in question. The similarity between the borophene/GaN and borophene/ZnO heterostructures also extends to the nature of the change in the Re $\dot{\varepsilon}$ and Im $\dot{\varepsilon}$ values with different light polarization directions. Therefore, in respect to the borophene/ZnO heterostructure, it can be also said that there is an anisotropy of the permittivity.

To explain the features of the change in the dielectric constant of the borophene/GaN and borophene/ZnO heterostructures in the considered wavelength range, including the establishment of the causes of anisotropy, the patterns of formation of the spectral profile of Re $\dot{\varepsilon}$ and Im $\dot{\varepsilon}$ of both structures were studied. Fig. 4 and 5 show the Re $\dot{\varepsilon}$ and Im $\dot{\varepsilon}$ profiles of the borophene/GaN heterostructure and its constituent 2D monolayers for the cases of polarization along the *X* axis and the *Y* axis, respectively. It follows from Fig. 4 that in the direction of the *X* axis the formation of permittivity profile is contributed decisively by the GaN monolayer. At the same time, in the case of the borophene/GaN heterostructure the characteristic peak of the Re $\dot{\varepsilon}$ and Im $\dot{\varepsilon}$ graphs of the GaN monolayer in the UV radiation range shifts to the interface between visible range and IR range, which can be explained by the influence of the borophene monolayer acting as a substrate for GaN. In the direction of the *Y* axis (Fig. 5), the role of borophene monolayer in the formation of the Re $\dot{\varepsilon}$ and Im $\dot{\varepsilon}$ profiles of the borophene/GaN heterostructure becomes more noticeable, but only within the UV and visible ranges. In particular, the effect of this monolayer explains the peak in the mid-UV range and the decreasing behavior of the Re $\dot{\varepsilon}$ and Im $\dot{\varepsilon}$ dependences in the visible radiation range.

Re $\dot{\varepsilon}$ and Im $\dot{\varepsilon}$ spectral profiles of the borophene/ZnO heterostructure and its constituent 2D monolayers for the cases of polarization along the *X* axis and the *Y* axis are shown in Fig. 6 and 7, respectively. The analysis of the calculated data presented in the figures shows that the manifestation of the synergistic effect from the combination of borophene and ZnO monolayers in the composition of a vertical heterostructure is the presence of an increasing portion of the Re $\dot{\varepsilon}$ and Im $\dot{\varepsilon}$ characteristics in the IR range for both directions of light polarization. The values of Re $\dot{\varepsilon}$ and Im $\dot{\varepsilon}$ remain almost unchanged on the characteristics of borophene and ZnO monolayers in the IR range, and Im $\dot{\varepsilon}$ has values close to zero. In the UV and visible ranges, the formation of the Re $\dot{\varepsilon}$ and Im $\dot{\varepsilon}$ profiles in the direction of the *X* axis is mainly contributed by ZnO, and in the direction of the *Y* axis it is mainly contributed by borophene. The appearance of a synergistic effect in the case of borophene/ZnO heterostructure rather than anywhere else can be explained by the following causes:

1) The monolayers of borophene and ZnO are located closer to each other (2.51 Å) in the direction of the *Z* axis (not periodic) in the composition of the supercell compared to the distance between the monolayers of borophene and GaN (2.91 Å). Differences between the distances along

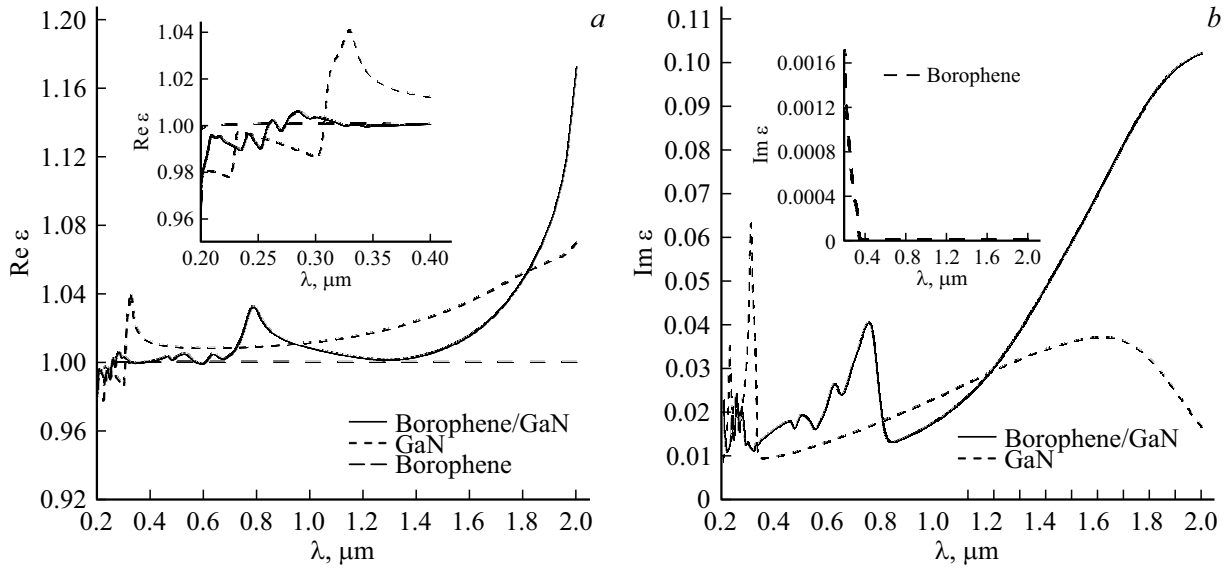

Figure 4. Spectral profile of the complex permittivity $\dot{\varepsilon}$ of the borophene/GaN heterostructure when the light is polarized along the X axis: (a) Re$\dot{\varepsilon}$; (b) Im $\dot{\varepsilon}$.

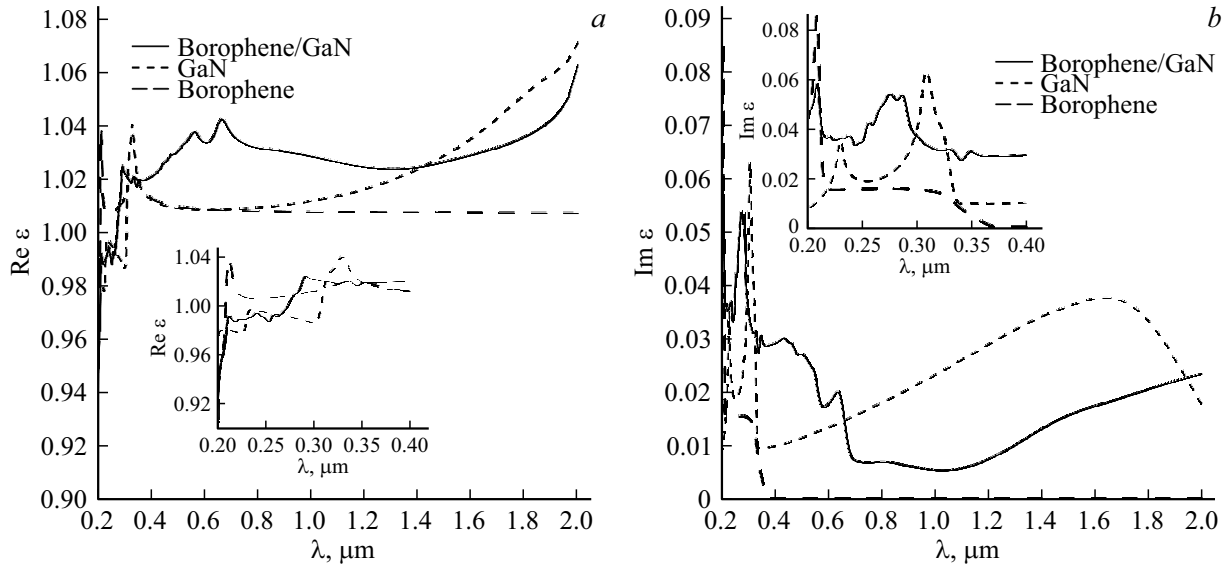

Figure 5. Spectral profile of the complex permittivity $\dot{\varepsilon}$ of the borophene/GaN heterostructure when the light is polarized along the Y axis: (a) Re ε; (b) Im ε.

the Z axis result in a noticeable difference in dihedral angles: in the case of GaN monolayer this value is negative and amounts to -7.21, and in the case of ZnO monolayer it is positive and amounts to 19.18. Due to these differences, the interaction between layers in the composition of the borophene/ZnO heterostructure will be more noticeable, which will lead to more noticeable changes in the properties of the heterostructure compared to the properties of its constituent monolayers.

2) Monolayers of GaN and ZnO have differences at the level of the band structure: GaN has an indirect band gap [41], and ZnO has a direct band gap [42]. Also, there are differences between them in the size of the band gap [43–45].

Let us turn to the analysis of the absorption spectra of the borophene/GaN and borophene/ZnO heterostructures shown in Fig. 8. It can be seen that both heterostructures are characterized by an anisotropy of the absorption coefficient when choosing the direction of light polarization, which manifested itself earlier in the Im $\dot{\varepsilon}$ graphs. It can be noted that the absorption peak for both heterostructures is in the UV range, which is explained by the significant contribution of borophene in the case of light polarization along the Y axis and the contribution of the ZnO monolayer

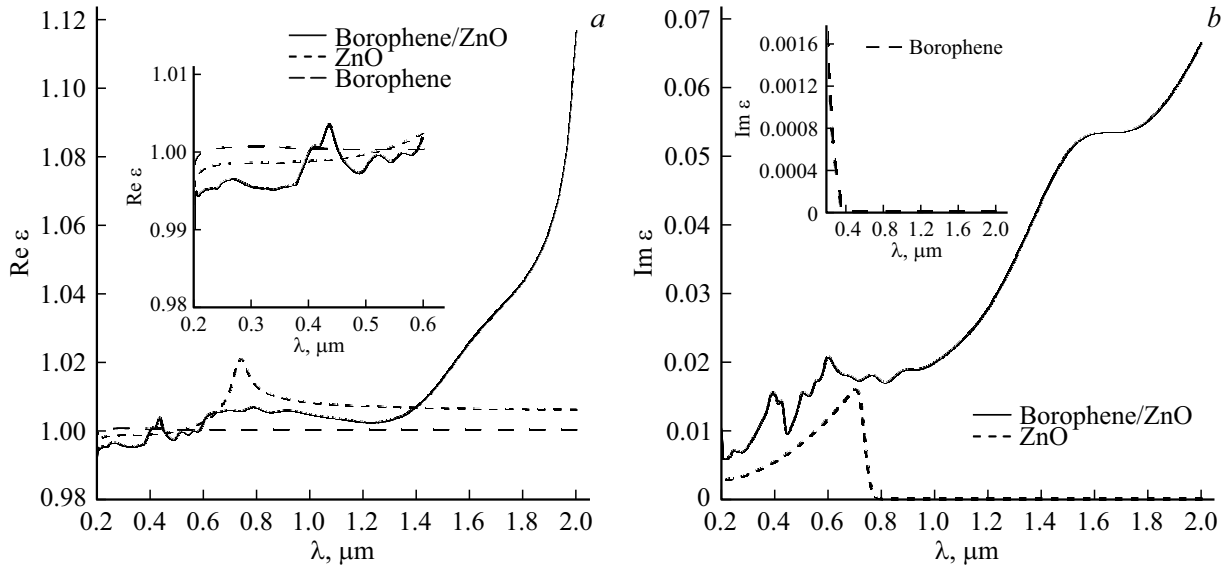

Figure 6. Spectral profile of the complex permittivity $\dot{\varepsilon}$ of the borophene/ZnO heterostructure when the light is polarized along the X axis: (a) Re $\dot{\varepsilon}$; (b) Im $\dot{\varepsilon}$.

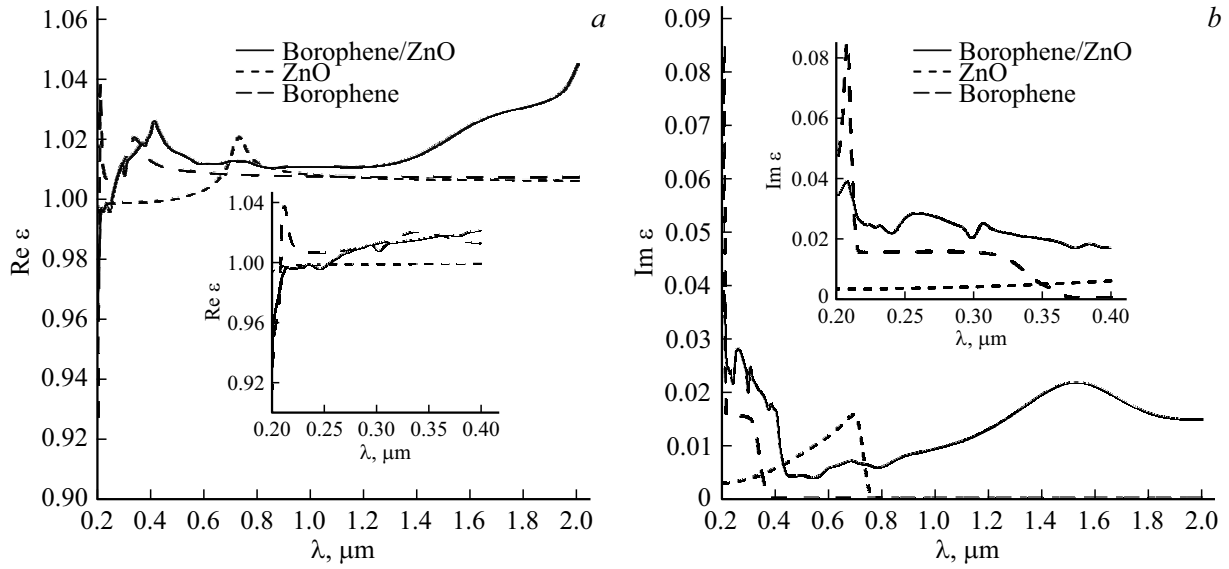

Figure 7. Spectral profile of the complex permittivity $\dot{\varepsilon}$ of the borophene/ZnO heterostructure when the light is polarized along the Y axis: (a) Re $\dot{\varepsilon}$; (b) Im$\dot{\varepsilon}$.

in the case of light polarization along the X axis. In the IR range, the absorption coefficient is small and does not exceed 3–4% in both directions of light polarization, which is explained by the small Im $\dot{\varepsilon}$ of borophene, GaN, and ZnO monolayers in this range of wavelengths. The difference in the values of the absorption coefficient of the borophene/GaN heterostructure between the UV and visible ranges can by as high as ~ 7 times, and between the UV and near-IR ranges it can be ~ 14 times. For the borophene/ZnO heterostructure, this difference can be up to ~ 6 times and up to ~ 18 times, respectively. The high sensitivity to electromagnetic radiation in the UV range compared to the sensitivity in the visible and near-IR ranges suggests that UV radiation detectors can be developed on the basis of vertical borophene/GaN and borophene/ZnO heterostructures.

5. Conclusion

Based on the results of the performed *ab initio* study, the following conclusions can be made. The considered atomic configurations of borophene/GaN and borophene/ZnO van der Waals heterostructures in the wavelength range of $0.2-2\,\mu$m manifest themselves as media with dielectric

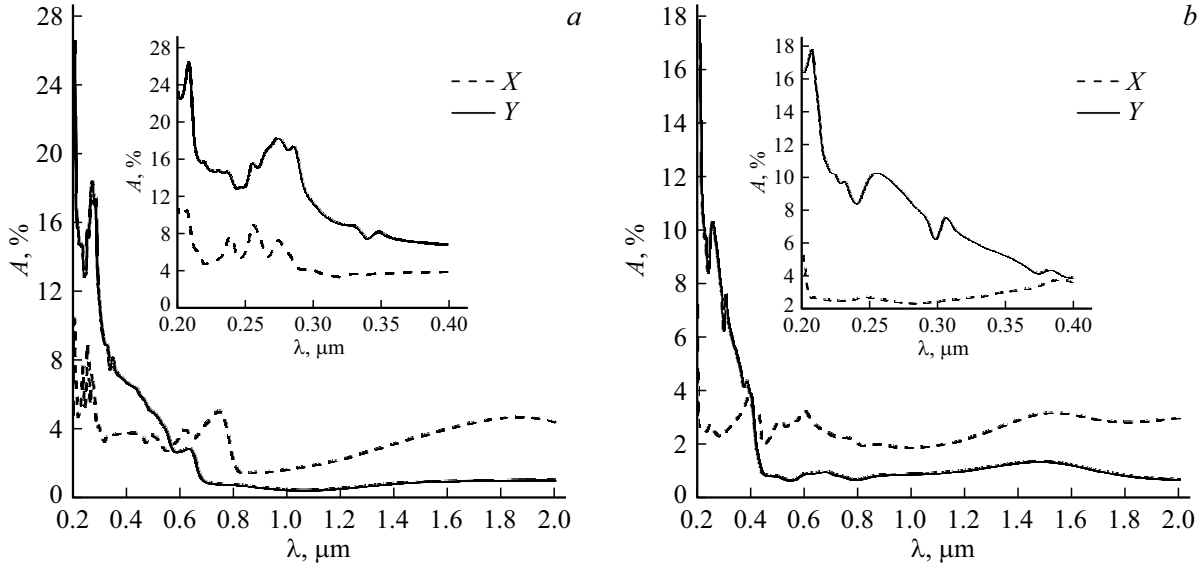

Figure 8. Absorption coefficient of borophene/GaN (*a*) and borophene/ZnO (*b*) heterostructures for light polarization along the *X* and *Y* axes.

properties. Each of the heterostructures, when choosing the direction of light polarization (along the edge of the zigzag shape of the GaN/ZnO monolayers, i.e. the *X* axis, along the edge of the zigzag shape of the borophene monolayer, i.e. the *Y* axis), is characterized by an anisotropy of the permittivity and absorption coefficient due to the different degree of the influence of monolayers that make up the heterostructure: when the light is polarized in the direction of the *X* axis, the semiconductor GaN and ZnO monolayers make a decisive contribution to the optical properties of the heterostructures, while in the direction of the *Y* axis the borophene monolayer with metallic conductivity makes the decisive contribution. Both heterostructures demonstrate high sensitivity to UV radiation, which makes them potentially promising materials for the development of UV detectors in the middle and far ranges. It is predicted that the efficiency of such detectors will be high because both heterostructures have low sensitivity to other wavelengths.

Funding

The work has been funded by a grant of the Russian Science Foundation (project № 21-72-00082), https://rscf.ru/project/21-72-00082/.

Conflict of interest

The authors declare that they have no conflict of interest.

References

[1] A.K. Geim, I.V. Grigorieva. Nature, **499**, 419 (2013). DOI: 10.1038/nature12385
[2] K.S. Novoselov, A. Mishchenko, A. Carvalho, A.H. Castro Neto. Science, **353**, aac9439 (2016). DOI: 10.1126/science.aac94
[3] J. Yao, G. Yanga. J. Appl. Phys., **131**, 161101 (2022). DOI: 10.1063/5.0087503
[4] L. Britnell, R.V. Gorbachev, R. Jalil, B.D. Belle, F. Schedin, A. Mishchenko, T. Georgiou, M.I. Katsnelson, L. Eaves, S.V. Morozov, N.M. Peres, J. Leist, A.K. Geim, K.S. Novoselov, L.A. Ponomarenko. Science, **335**, 947 (2012). DOI: 10.1126/science.1218461
[5] C.C. Chen, Z. Li, L. Shi, S.B. Cronin. Nano Res., **8**, 666 (2015). DOI: 10.1007/s12274-014-0550-8
[6] C.E. Ekuma, S. Najmaei. ACS Appl. Nano Mater., **3**, 7136 (2020). DOI: 10.1021/acsanm.0c01465
[7] W. Choi, N. Choudhary, G.H. Han, J. Park, D. Akinwande, Y.H. Lee. Mater. Today, **20**, 116 (2017). DOI: 10.1016/j.mattod.2016.10.002
[8] Z. Kang, Y. Ma, X. Tan, M. Zhu, Z. Zheng, N. Liu, L. Li, Z. Zou, X. Jiang, T. Zhai, Y. Gao. Adv. Electron. Mater., **3**, 1700165 (2017). DOI: 10.1002/aelm.201700165
[9] X. Kong, Q. Liu, C. Zhang, Z. Peng, Q. Chen. Chem. Soc. Rev., **46**, 2127 (2017). DOI: 10.1039/C6CS00937A
[10] Y. Liu, N.O. Weiss, X. Duan, H.-C. Cheng, Y. Huang, X. Duan. Nat. Rev. Mater., **1**, 16042 (2016). DOI: 10.1038/natrevmats.2016.42
[11] X. Zhou, X. Hu, J. Yu, S. Liu, Z. Shu, Q. Zhang, H. Li, Y. Ma, H. Xu, T. Zhai. Adv. Funct. Mater., **28**, 1706587 (2018). DOI: 10.1002/adfm.201706587
[12] S. Liang, B. Cheng, X. Cui, F. Miao. Adv. Mater., **32**, 1903800 (2019). DOI: 10.1002/adma.201903800
[13] M.Z. Bellus, M. Li, S.D. Lane, F. Ceballos, Q. Cui, X.C. Zeng, H. Zhao. Nanoscale Horiz., **2**, 31 (2017). DOI: 10.1039/C6NH00144K
[14] X. Hong, J. Kim, S.-F. Shi, Y. Zhang, C. Jin, Y. Sun, S. Tongay, J. Wu, Y. Zhang, F. Wang. Nature Nanotech., **9**, 682 (2014). DOI: 10.1038/nnano.2014.167
[15] K. Zhang, T. Zhang, G. Cheng, T. Li, S. Wang, W. Wei, X. Zhou, W. Yu, Y. Sun, P. Wang, D. Zhang, C. Zeng, X. Wang, W. Hu, H.J. Fan, G. Shen, X. Chen, X. Duan, K. Chang, N. Dai. ACS Nano, **10**, 3852 (2016). DOI: 10.1021/acsnano.6b00980

[16] Y. Zou, Y. Zhang, Y. Hu, H. Gu. Sensors, **18**, 2072 (2018). DOI: 10.3390/s18072072
[17] L. Peng, Y. Cui, L. Sun, J. Du, S. Wang, S. Zhang, Y. Huang. Nanoscale Horiz., **4**, 480 (2019). DOI: 10.1039/C8NH00413G
[18] W.X. Zhang, Y. Yina, C. He. Phys. Chem. Chem. Phys., **22**, 26231 (2020). DOI: 10.1039/D0CP04474A
[19] Y. Zhu, K. Liu, Q. Ai, Q. Hou, X. Chen, Z. Zhang, X. Xie, B. Lia, D. Shen. J. Mater. Chem. C, **8**, 2719 (2020). DOI: 10.1039/C9TC06416H
[20] Z. Liu, X. Wang, Y. Liu, D. Guo, S. Li, Z. Yan, C.-K. Tan, W. Li, P. Li, W. Tang. J. Mater. Chem. C, **7**, 13920 (2019). DOI: 10.1039/C9TC04912F
[21] L. Yu, Y.H. Lee, X. Ling, E.J. Santos, Y.C. Shin, Y. Lin, M. Dubey, E. Kaxiras, J. Kong, H. Wang, T. Palacios. Nano Lett., **14**, 3055 (2014). DOI: 10.1021/nl404795z
[22] K. Zhang, T. Zhang, G. Cheng, T. Li, S. Wang, W. Wei, X. Zhou, W. Yu, Y. Sun, P. Wang, D. Zhang, C. Zeng, X. Wang, W. Hu, H.J. Fan, G. Shen, X. Chen, X. Duan, K. Chang, N. Dai. ACS Nano, **10**, 3852 (2016). DOI: 10.1021/acsnano.6b00980
[23] S. Kaur, A. Kumar, S. Srivastava, K. Tankeshwar. Phys. Chem. Chem. Phys., **19**, 22023 (2017). DOI: 10.1039/C7CP03960C
[24] A.J. Mannix, X.-F. Zhou, B. Kiraly, J.D. Wood, D. Alducin, B.D. Myers, X. Liu, B.L. Fisher, U. Santiago, J.R. Guest, M.J. Yacaman, A. Ponce, A.R. Oganov, M.C. Hersam, N.P. Guisinger. Science, **350**, 1513 (2015). DOI: 10.1126/science.aad1080
[25] N. Katoch, A. Kumar, R. Sharma, P.K. Ahluwalia, J. Kumar. Phys. E: Low-Dimens. Syst. Nanostructures, **2020**, 120, 113842. DOI: 10.1016/j.physe.2019.113842
[26] S. Jing, W. Chen, J. Pan, W. Li, B. Bian, B. Liao, G. Wang. Mater. Sci. Semicond. Process., **146**, 106673 (2022). DOI: 10.1016/j.mssp.2022.106673
[27] J.W. Jiang, X.C. Wang, Y. Song, W.B. Mi. Appl. Surf. Sci., **440**, 42 (2018). DOI: 10.1016/j.apsusc.2018.01.140
[28] J.M. Soler, E. Artacho, J.D. Gale, A. García, J. Junquera, P. Ordejón, D. Sánchez-Portal. J. Phys.: Condens. Matt., **14**, 2745 (2002). DOI: 10.1088/0953-8984/14/11/302
[29] J.P. Perdew, J.A. Chevary, S.H. Vosko, K.A. Jackson, M.R. Pederson, D.J. Singh, C. Fiolhais. Phys. Rev. B, **46**, 6671 (1992). DOI: 10.1103/PhysRevB.46.6671
[30] S. Grimme. J. Comput. Chem., **27**, 1787 (2006). DOI: 10.1002/jcc.20495
[31] H.J. Monkhorst, J.D. Pack. Phys. Rev. B, **13**, 5188 (1976). DOI: 10.1103/PhysRevB.13.5188
[32] P. Pulay. Chem. Phys. Lett. **73**, 393 (1980). DOI: 10.1016/0009-2614(80)80396-4
[33] E.N. Economou. *Green's Functions in Quantum Physics*, 3rd ed. (Springer, Berlin, 1983), p. 55−75. DOI: 10.1007/3-540-28841-4_4
[34] *The Materials Project*. [Electronic source]. URL: https://materialsproject.org/.
[35] Z. Deng, X. Wang, J. Cui. RSC Adv., **9**, 13418 (2019). DOI: 10.1039/C9RA01576K
[36] J. Wu, M. Gong. J. Appl. Phys., **130**, 070905 (2021). DOI: 10.1063/5.0060255
[37] Z. Luo, X. Fan, Y. An. Nanoscale Res. Lett., **12**, 514 (2017). DOI: 10.1186/s11671-017-2282-7
[38] Z. Zhang, E.S. Penev, B.I. Yakobson. Chem. Soc. Rev., **46**, 6746 (2017). DOI: 10.1039/C7CS00261K
[39] M. Idrees, C.V. Nguyen, H.D. Bui, I. Ahmad, B. Amin. Phys. Chem. Chem. Phys., **22**, 20704 (2020). DOI: 10.1039/D0CP03434G
[40] X. Gao, Y. Shen, Y. Ma, S. Wu, Z. Zhou. J. Mater. Chem. C, **7**, 4791 (2019). DOI: 10.1039/C9TC00423H
[41] H. Xiang, H. Quan, Y. Hu, W. Zhao. J. Inorg. Mater., **36**, 492 (2021). DOI: 10.15541/jim20200346
[42] K. Ren, J. Yu, W. Tang. J. Alloys Compd.,**812**, 152049 (2020). DOI: 10.1016/j.jallcom.2019.152049
[43] S. Xia, Y. Diao, C. Kan. J. Colloid Interface Sci., **607**, 913 (2022). DOI: 10.1016/j.jcis.2021.09.050
[44] G. Wang, W. Tang, L. Geng, Y. Li, B. Wang, J. Chang, H. Yuan. Phys. Status Solidi B, **257**, 1900663 (2019). DOI: 10.1002/pssb.201900663
[45] Y. Zhang, M. Zhang, Y. Zhou, J. Zhao, S. Fang, F. Li. J. Mater. Chem. A, **2**, 13129 (2014). DOI: 10.1039/C4TA01874E

Translated by Y.Alekseev